SLAC-PUB-2501
April 1980
(M)

SURFACE PENNING IONIZATION OF THE CO-COVERED Pd(111) SURFACE BY METASTABLE HELIUM (2^1S, 2^3S)-BEAMS *

Sheng-Wei Wang

Stanford Linear Accelerator Center, Stanford Univ., Stanford, CA 94305 USA.

H. Conrad, G. Ertl, J. Küppers,

Univ. München, Inst. für Physikalish Chemie, W. Germany.

G. Haberland,

Univ. Freiburg, Fakultät für Physik, W. Germany.

Abstract

Surface Penning ionization (SPI) in the process

$$He^*(2^1S,\ 2^3S) + CO \rightarrow He(1^1S) + CO^+ + e^-$$

is investigated theoretically for CO molecules chemisorbed on a Pd(111) surface at low collision energy of metastable He^*-beams. The actual process can well be explained in terms of Auger deexcitation. The entire SPI process occurs at the topmost layer, thereby increasing the surface sensitivity. The potential energy surfaces between the collision partners in the initial and final states are calculated using the local spin density functional formalism. The angle distribution and ionization rate of emitted electrons are calculated based on the Golden Rule, assuming CO standing straight on the substrate for various impact geometries. Pronounced "shadow" effect due to neighboring CO molecules at grazing He^* incident angles and in the emitted electron angle distributions is obtained. Comparisons with experimental data are made. Our results exhibit the usefulness of SPI in studying the electronic and geometrical structure of adsorbates on surfaces.

In a previous paper {1} (referred to as I) energy distributions of electrons ejected from clean and CO-covered Pd(111) surfaces by impact with metastable He^*2^1S (excitation energy E^*=20.6 eV) and 2^3S(E^*=19.8 eV) have been reported. These results have been verified both experimentally and theoretically as due to the operation of the Penning ionization (=Auger deexcitation) mechanism, via

$$He^* + CO/Pd(111) \rightarrow He + CO^+/Pd(111) + e^- \quad . \qquad (1)$$

Recently a first theoretical analysis {2} (referred to as II) of surface Penning ionization (SPI) appeared in which the potential energy curves, ionization rates and angle distributions of the emitted electrons for the same system were obtained. The results of this analysis can be summarized as follows:

(1) The well depths of the interaction potential energy curves between the collision partners in the initial and final states are both very small and indicate a "hard core" type collision process. The ionization rate $\Gamma(\vec{R})$ decays exponentially as a function of O···He^* internuclear separation. This means that most of the ionization events take place at the classical turning point $\vec{R}m$ between the collision partners and it is a reasonable approximation to assume the ionization transition to occur only at Rm.

(2) The angle distribution for electrons emitted from an isolated CO molecule with a single He^* at $\vec{R}m$ is written in partial wave expansion as

$$\Gamma_{\vec{k}}(\vec{R}m,\gamma) = 2\pi\rho_{E_{\vec{k}}} \left| \sum_{\ell=0}^{\infty} P_\ell(\cos\gamma)\, i^{-\ell}\, e^{i\delta_\ell}\, I_\ell(\vec{R}m) \right|^2 \qquad (2)$$

*Supported in part by Dept. of Energy, contract DE-AC03-76SF00515, and by DFG. Presented at the 8th Int. Vacuum Congress - 4th Int. Conf. on Solid Surfaces - 3rd European Conf. on Surface Science, Cannes, France, September 22-26, 1980.

where

$$I(\vec{R}m) \approx S_1(\vec{R}m) \cdot S_2(|\vec{R}m|) / |\vec{R}m|$$

P_ℓ is the usual Legendre polynomial and δ_ℓ is the phase shift for the ℓth partial wave. S_1 is the overlap between the CO orbitals and the HelS orbital (defined in II). S_2^ℓ is the overlap between the ℓth partial wave of the continuum orbital and the He^*2S orbital. Γ is asymmetric with respect to $\gamma = \pi/2$ (Fig. 3a of II), where γ is the polar angle with respect to the $O\cdots He^*$ axis. This is due to the interferences of the partial waves contained in the final state effect (the S_2^ℓ term). The initial state effect reduces to $S_1(\vec{R}m)$ which depends on $\vec{R}m$, but not on the emission angle γ.

(3) The intensity $I(\theta_D, \phi_D)$ at the detector measured with respect to the He^* incident direction (θ_{He^*}, ϕ_{He^*}, with respect to the surface normal) has to be averaged over all the allowed impact geometries. This gives

$$I(\theta_D, \phi_D) = \iint \Gamma_{\vec{k}}(\theta_D, \theta_M, \phi_M)\, b\,db\, d\phi_M \qquad (3)$$

The integration ranges over the unshadowed parts of the surface atoms. $\{\theta_M, \phi_M\}$ are the polar and azimuthal angles of the $O\cdots He^*$ axis with respect to the vector of the relative velocity. The substitution

$$\cos\gamma = \pm\sin\theta_D \sin\theta_M \cos\phi_M + \cos\theta_D \cos\theta_M$$

has been made in (3) for Γ to transform quantities calculated within the molecular frame into those within the relative velocity frame. Here '+' sign is for $\phi_D = 0^o$ and '-' sign for $\phi_D = 180^o$.

(4) In II no "cast shadows" were considered, but the impact parameter on any given molecule was limited due to the neighboring molecules. This was a good approximation near normal incidence, where there are no cast shadows. At grazing angles the cast shadows are important and require a better treatment. The description in (1)-(4) forms the starting point for a rigorous discussion of the emitted electron angle distribution. However one must realize that the biggest difference between the gas phase PI and SPI is the effect of the adsorbate overlayer structures on the surface and the influence of neighboring CO's on each other, i.e., the "shadow" effect produced by the previous CO before the He^* hits the next CO. We shall discuss this effect in great detail and the resulting electron angle distributions derived from it.

Fig. 1 shows the two He^* incident azimuths chosen here along the atomic chains formed by O atoms. At normal incidence, all the impact events enclosed by the circle are included and at off-normal incidence the unshadowed area for each CO will be included. 3-dimensional views along the incidence direction 54° at these two incident azimuths are shown in Fig. 2(a) and 2(a'). For illustrative purposes, we show in the lower graph of Fig. 2 a 1-dimensional plot of the He^* trajectories (assuming a straight line trajectory) which are tangential lines to the hypothetical circles formed by $O\cdots He^*$ at the classical turning point radius at $\theta_{He^*} =$ 84°, 74°, 64° and 54°. The heavy lines indicate the unshadowed portions for each CO. We also indicate that along one of these tangential lines, He^* is close enough to interact with two CO molecules simultaneously. However, this complication will not be discussed here.

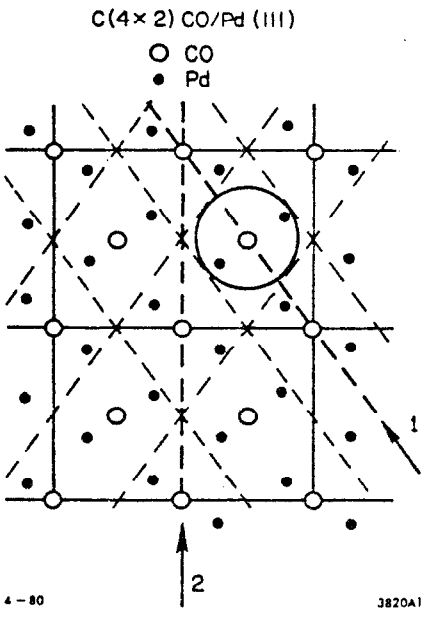

Fig. 1 - C(4 x 2) CO overlayer structure on Pd(111) (coverage $\theta = 0.5$). Arrows 1 and 2 denote the He^* incident azimuths.

Fig. 2 - Unshadowed surface area at $\theta_{He}^* = 54^o$. (a) for azimuth 1 and (a') for 2. The lower figure is for the 1-dimensional case.

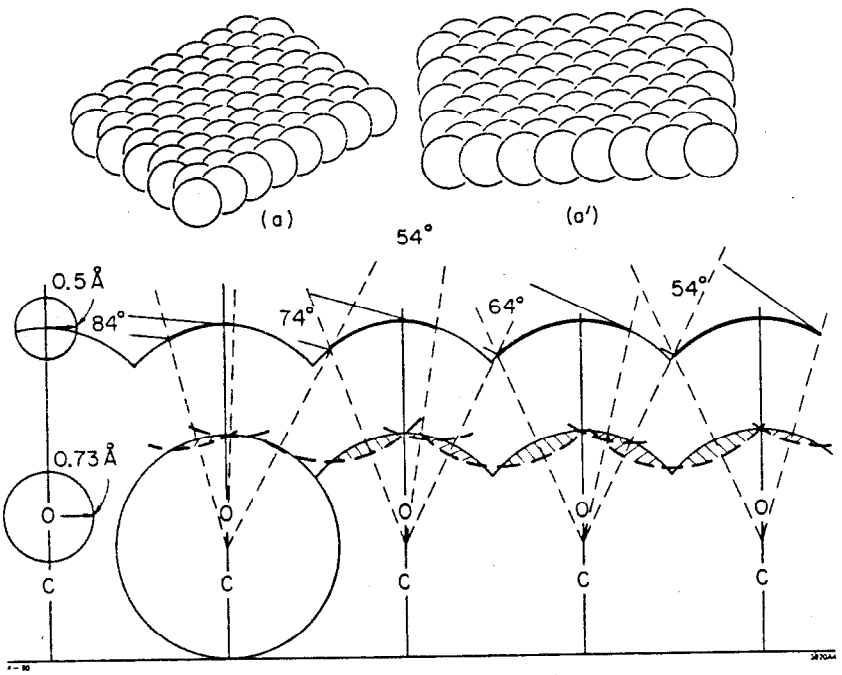

In Fig. 3, E_k marks the measured electron kinetic energy distributions at various emitting polar angles and E_F marks the effective binding energies of these electrons with respect to the Fermi level of the surface. $E_B \sim 8.4$ and ~ 11.3 eV correspond to the $(5\sigma + 1\pi)$ and 4σ

Fig. 3 - Experimental energy distribution spectrum of the emitted electrons at various detecting angles.

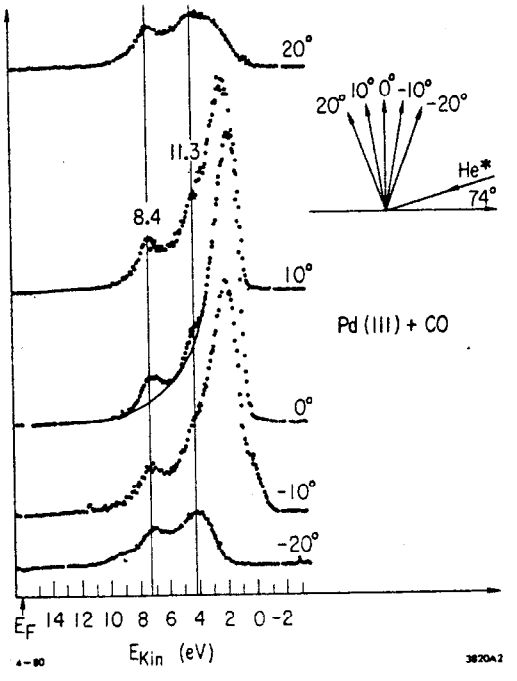

Fig. 4 - Theoretical (curve 1) experimental (in dots) angular patterns for $\theta_{He}^* = 54^o$ and 64^o. Curve 2 is the rotated curve 1 by about 20^o.

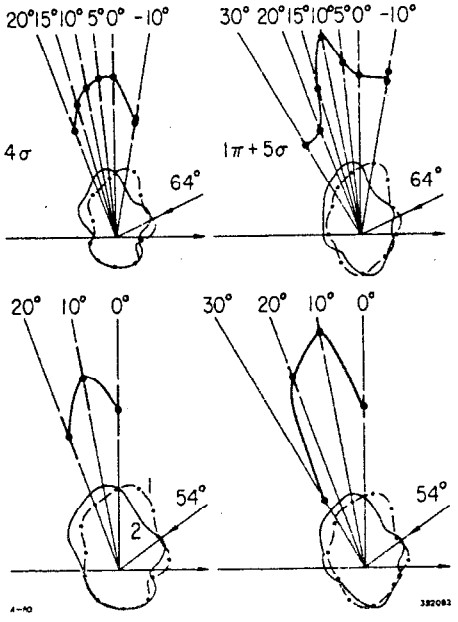

levels of CO. Electron emission near the threshold has been explained in II as due to the secondary electrons. We show in the zero-degree spectrum how the secondary electron contribution is subtracted. The integral of the peak above this curve is our intensity.

Figure 4 shows the results of the theoretically calculated electron angle distributions (curve 1) for the 4σ and $(5\sigma + 1\pi)$ orbitals and the experimental data (indicated

by dots, at an unknown incident azimuth). The theoretical results are obtained by using (3) with the appropriate impact parameters and Γ for the 3-dimensional case but leave out the corner effects shown in Fig. 1. (area outside the circle but enclosed by the parallellogram). One first notices that the angular patterns are much smoother than those obtained in II since most of the intensity variations smear out as a result of the more complete 3-dimensional averaging procedures. $I(\theta_D)$ is asymmetric with respect to $\theta_D=\pi/2$ and has most of its intensity in the backward direction toward the incident He^* beam. This is similar to what has been called the "shadow" effect in the electron angular distribution described in II.

The comparison between theoretical results and experimental data seems encouraging considering the various approximations used in the theory and the experimental uncertainties. A better agreement can be seen by rotating the angular pattern away from the incident angle by $\Delta\theta \sim 20^o$. However its implication can not be offered at this moment. There are several steps which can be taken on the theoretical side to make further investigations and these are:

(1) The He^* atoms do not strictly follow a straight line trajectory since the $He^*\cdots OC$ potentials have both attractive and repulsive parts. Calculations of He^* deflection functions can be carried out within the classical binary collision theory {3}. This will enable a better determination of the actual He^* incident angle near the classical turning point.

(2) The corner effect neglected in the averaging procedure can be included at normal He^* incidence and can produce appreciable intensity variations (results will be shown in another publication) {4}. At off-normal incidence, these corner effects may be reduced since then the areas of the corners are relatively smaller. The inclusion of them for off-normal incidence in the 3-dimensional case is a difficult task and remains yet to be solved.

(3) When a He^* atom is at the closest approach with two neighboring CO's the emitted electron intensity should be the weighted sum of these two contributions. The importance of this complication should be examined as a next step.

(4) At large angle of incidence (near grazing) each He^* interacts with many surface atoms and goes through a multiple scattering trajectory {3} producing more pronounced interference patterns due to all the surface atoms. This effect may explain the multiple peaks observed at $\theta_{He^*} = 84^o$ for the $5\sigma + 1\pi$ emission (not shown). To avoid this complication, smaller incident angles are recommended in future experimental work.

Finally, electron multiple scattering effects which have been observed in many other kinds of experiment, such as photoemission, low-energy electron diffraction and electron energy loss spectroscopy, may also play a role in SPI. However, we expect these effects to be probably much weaker in SPI, because of the strongly outward peaked electron emission at fixed impact parameter (see Fig. 3(a) in II). The inward emission will not be able to affect the strong outward emission substantially through multiple scattering, because it is weak and widely directed. Averaging over impact parameters does not change this result, but does reduce the apparent outward emission because the sharp peak sweeps around with changing impact parameters. This averaging broadens the outward emission, as is also seen in Fig. 4 in the absence of multiple scattering. The widely directed inward emission carries altogether a fair number of electrons that may be responsible for the secondary electron emission observed experimentally (see II).

References

*Supported in part by Dept. of Energy, contract DE-AC03-76SF00515, and by DFG.

1. H. Conrad, G. Ertl, J. Küppers, S. W. Wang, K. Gérard and H. Haberland, Phys. Rev. Letters 42, 1082 (1979).
2. S. W. Wang and G. Ertl, Surf. Sci. 93, L75 (1980).
3. E. S. Mashkova and V. A. Malchanov, Radiation Effects 16, 143 (1972).
4. S. W. Wang, to be published.